HHS Public Access

Author manuscript

Gastroenterology. Author manuscript; available in PMC 2019 April 01.

Published in final edited form as:

Gastroenterology. 2018 April ; 154(5): 1421–1434. doi:10.1053/j.gastro.2017.12.013.

Knockdown of Anillin Actin Binding Protein Blocks Cytokinesis in Hepatocytes and Reduces Liver Tumor Development in Mice without Affecting Regeneration

Shuyuan Zhang[1], **Liem H. Nguyen**[1], **Kejin Zhou**[2], **Ho-Chou Tu**[3], **Alfica Sehgal**[3], **Ibrahim Nassour**[1], **Lin Li**[1], **Purva Gopal**[4], **Joshua Goodman**[1], **Amit G. Singal**[5], **Adam Yopp**[6], **Yu Zhang**[1], **Daniel J. Siegwart**[2], and **Hao Zhu**[1,*]

[1]Children's Research Institute, Departments of Pediatrics and Internal Medicine, Center for Regenerative Science and Medicine, University of Texas Southwestern Medical Center, Dallas, TX 75390, USA

[2]Simmons Comprehensive Cancer Center, Department of Biochemistry, University of Texas Southwestern Medical Center, Dallas, TX 75390, USA

[3]Alnylam Pharmaceuticals, Inc., Cambridge, MA 02142, USA

[4]Department of Pathology, University of Texas Southwestern Medical Center, Dallas, TX 75390, USA

[5]Department of Internal Medicine, University of Texas Southwestern Medical Center, Dallas, TX 75390, USA

[6]Department of Surgery, University of Texas Southwestern Medical Center, Dallas, TX 75390, USA

Abstract

Background & Aims—Cytokinesis can fail during normal post-natal liver development, leading to polyploid hepatocytes. We investigated whether inhibiting cytokinesis in the liver slows tumor growth without compromising the health of normal hepatocytes. We inhibited cytokinesis in cancer cells by knocking down anillin actin binding protein (ANLN), a cytoskeletal scaffolding protein that regulates cytokinesis and might promote tumorigenesis, in mice with liver disease.

Methods—We analyzed clinical and gene expression data from The Cancer Genome Atlas, Oncomine, PrognoScan, and a hepatocellular carcinoma (HCC) tissue microarray. We knocked down ANLN with small interfering RNAs (siRNAs) in H2.35 liver cells and performed image

*Correspondence to: Hao Zhu, Hao.Zhu@utsouthwestern.edu, Phone: (214) 648-2850.

Author contributions

S.Z. and H.Z. conceived the project, performed the experiments and wrote the manuscript. I.N., J.G., L.L., S.Z., and L.N., assisted with experiments and mouse work. K.Z. and D.S. assisted with the chemistry experiments. A.S., A.Y. helped with human HCC tissue microarray. Y.Z. helped to generate the *TG-shAnln* mouse model.

The authors whose names are listed certify that they have NO conflict of interest.

analyses of cells undergoing cytokinesis. siRNAs were delivered to LAP-MYC mice, which develop hepatoblastoma, using lipid nanoparticles. H2.35 cells with knockdown of ANLN or control cells were injected into FRG mice, which develop chronic liver damage, and tumor growth was monitored. We also developed mice with inducible expression of transgenes encoding small hairpin RNAs (shRNAs) against *Anln* mRNA and studied liver tumorigenesis following administration of diethylnitrosamine and carbon tetrachloride. siRNAs against *Anln* mRNA were conjugated to N-acetylgalactosamine to reduce toxicity and increase hepatocyte tropism; their effects were studied in mouse models of liver cancer and regeneration.

Results—Levels of *ANLN* mRNA were increased in human HCC tissues compared to non-tumor liver tissues. siRNA knockdown of ANLN blocked cytokinesis in H2.35 liver cells. Administration of siRNA against ANLN increased survival times of LAP-MYC mice, compared to mice given a control siRNA. H2.35 liver cells with shRNA knockdown of ANLN formed tumors more slowly in FRG mice than control H2.35 cells. Mice with inducible expression of shRNAs against *Anln* mRNA developed fewer liver tumors after administration of diethylnitrosamine and carbon tetrachloride than control mice. Knockdown of ANLN did not affect liver regeneration after acute and chronic liver injuries.

Conclusions—Knockdown of ANLN in liver cells blocks cytokinesis and inhibits development of liver tumors in mice. Agents that inhibit ANLN in the liver might be effective for prevention or treatment of HCC.

Graphical Abstract

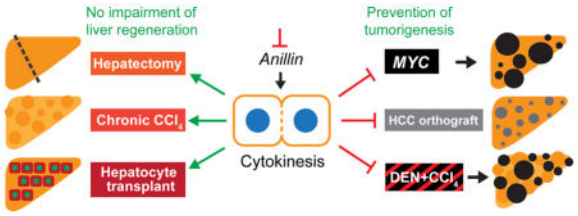

Keywords

RNA interference; hepatic carcinogenesis; cell cycle; tumorigenesis

INTRODUCTION

Cytokinesis is essential for complete cell division and is a process shared by most mitotic cells[1]. Thus, inhibiting cytokinesis to treat cancer could lead to detrimental outcomes for normal tissues containing cells that undergo repeated cell division[2–5]. In contrast, the liver uniquely undergoes cytokinesis failure to generate polyploid cells as part of its normal postnatal development process[6–8]. More than 50% of adult rodent hepatocytes are polyploid, harboring four or more copies of chromosomes in their nuclei, as opposed to 2c diploid cells[9–11]. It is likely that human hepatocytes also undergo cytokinesis failure during liver maturation[6, 12, 13]. Given this tolerance for cytokinesis failure, we hypothesized that the liver would be amenable to cytokinesis inhibition as an anti-cancer strategy.

Previously, it was shown that livers without *Cdk1*, a critical cyclin dependent kinase and mediator of cytokinesis, developed normally and was able to regenerate after partial hepatectomy[14]. These livers had enlarged hepatocytes that were massively polyploid due to cell cycle abnormalities and incomplete cytokinesis. Moreover, these liver-deficient *Cdk1* mice developed less cancer after diethylnitrosamine (DEN) mutagen treatment[14]. However, that study did not address whether cytokinesis failure could be tolerated in the context of chronic injuries that demand long-term regeneration and tissue restoration. This is an essential point as hepatocellular carcinoma (HCC), the most common form of primary liver malignancy, occurs most commonly in the setting of long-term chronic damage, such as alcohol use or viral hepatitis. In addition, it is not clear if cytokinesis inhibition would prevent cancer proliferation in a cell autonomous fashion or promote cancer development by worsening a damaged tissue microenvironment in a non-cell autonomous fashion.

To interrogate the effects of cytokinesis in cancer formation, we targeted a protein that is specifically important for cytokinesis rather than one like CDK1, which influences all stages of mitosis. ANLN is an evolutionarily conserved actin binding protein that serves as a key mediator of cytokinesis[15, 16]. ANLN contains conserved N-terminal actin and myosin binding domains, a C terminus Anillin homology domain and a PH domain which binds to RhoA, Ect2, and Septins[16, 17]. ANLN binds to all three types of actin filaments[16, 18, 19] as well as other important cytoskeletal components, serving as a scaffolding protein to coordinate cytokinesis in space and time. The exact mechanisms by which ANLN functions in cytokinesis remains incomplete, but its presence is important during multiple stages of cytokinesis[20–22].

Previous studies suggested that *ANLN* overexpression contributes to human cancer growth and implicated ANLN as a potential therapeutic target. *ANLN* siRNA knockdown in breast cancer and non-small cell lung cancer (NSCLC) cell lines inhibits proliferation[23, 24]. Moreover, *ANLN* expression was shown to serve as an independent prognostic marker for breast cancer patients[25]. However, it is unknown if ANLN is required by normal or malignant hepatocytes for cytokinesis and cell division, and no study has investigated the role of ANLN in liver cancer development.

Here, we generated multiple methods and models for *Anln* inhibition that successfully induced cytokinesis failure. We then tested the effects of blocking *Anln* in multiple cancer models and found that *Anln* inhibition impaired tumor initiation and growth and could extend overall survival. Importantly, we found that *Anln* suppression did not contribute significantly to liver tissue damage, nor did it impair normal liver functions and the capacity to regenerate after both acute and chronic injuries. Collectively, these preclinical results in multiple endogenous liver cancer models suggest that inhibiting cytokinesis is a tolerable and effective HCC prevention strategy in the setting of liver damage.

METHODS

Mouse strains, breeding, and analysis

All mice were handled in accordance with the guidelines of the Institutional Animal Care and Use Committee at UTSW. *TG-shAnln* embryonic stem cells were targeted by the UTSW

Transgenic Core led by Robert Hammer and injected by the CRI Mouse Genome Engineering Core. The strategy was based on work from Scott Lowe's group[26]. Briefly, the *shAnln* sequences were cloned into the pCol-TGM vector (Addgene #32715) and electroporated into KH2 embryonic stem cells together with a Flpe plasmid. Validated KH2 clones were then injected into blastocysts to generate knockin transgenic mice. The inducible *LAP-MYC* mice were carried on a pure FVB strain background. All experiments were done in an age and sex controlled fashion unless otherwise noted in the figure legends. *FRG* mice and nitisinone (NTBC) were purchased from Yecuris Corporation (10-0001). All experiments were done in an age and sex controlled fashion unless otherwise noted in the figure legends. The experimental mice were randomized using a simple randomization method.

Cell culture experiments

The H2.35 cell line was obtained from ATCC and has been cultured for less than 6 months. The cells were authenticated by ATCC using Short Tandem Repeat (STR) DNA profiling. Cells were cultured in DMEM with 4% (vol/vol) FBS, 1x Pen/Strep (Thermo Scientific) and 200 nM Dexamethasone (Sigma). Cells were transfected with control (Life Technologies, #4404020), *Anln siRNA1* (Life Technologies, #4390771, S87033), *Anln siRNA2* (Life Technologies, #4390771, S87032), and *Anln siRNA3* (Life Technologies, #4390771, S87034) by RNAiMAX (Invitrogen) in a 6-well plate, 10pmol siRNA/well. Live cell imaging started at 36 hours after transfection, using a Deltavision pDV microscope to take pictures every 3min. For immunofluorescence, cells were fixed 3 days after transfection. The lentiviral shRNA construct (TRMPVIR) was obtained from Scott Lowe's group through Addgene [27]). For the growth curve assays, the scramble shRNA and Anln shRNA cell lines were plated in 12 well plates with 30000 cells/well and treated with doxycycline (1ug/mL). For the cell synchronization assay, H2.35 cells were synchronized at G2–M phase by a nocodazole block. Briefly, siRNA transfected cells were treated with 150ng/mL nocodazole (Sigma) at 36 hours after transfection for 8 hours. After releasing, cells were harvested by 4% PFA (Invitrogen) fixation in every 20 minutes, from 0 min until 140 min. Then the cells were subjected to immunofluorescence staining.

Chemical injury experiments

CCl_4 is diluted 1:10 in corn oil (Sigma), and administered IP at a dose of 0.5 ml/kg of mouse as described previously [28]. DEN (Sigma) is diluted in saline and administered IP at different doses, depending on mouse age. For P19 mice, 25μg/g of mouse was injected once; for P24–P27 mice, 75μg/g was injected once; for P34 mice, 100μg/g was injected once.

Partial hepatectomy

Two-thirds of the liver was resected as previously described[29].

Liver function tests

Blood samples (~50μl) were collected retro-orbitally in heparinized tubes. Liver function tests were performed by the UTSW Molecular Genetics Core.

Flow Cytometry

For detection of ploidy populations, transfected H2.35 cells (1×10^6/mL) or sh*Anln* cells were fixed in 75% ethanol at −20°C, then inc ubated with 500μL (2×10^6/mL) of PI/Rnase Staining Buffer (BD Pharmingen) at 25°C for 15 minutes. Cells were analyzed with a BD FACS Aria Fusion machine.

In vivo Anln siRNA experiments

For in vivo experiments in *LAP-MYC* mice, formulated 5A2-SC8 dendrimer lipid nanoparticles (LNPs) were used to package either Control (Life Technologies, #4457289) or *Anln siRNA* (Life Technologies, #4457308, s87033) at 2 mg/kg, two times a week for a total of 5 doses (2 intraperitoneal and 3 retro-orbital). LNPs containing siRNAs were formulated following the previously reported component ratios of 5A2-SC8, DSPC, cholesterol, and lipid PEG2000 (molar ratio of 50:38:10:2) and methods[30] with the aid of a microfluidic rapid mixing instrument (Precision Nanosystems NanoAssemblr) and purified by dialysis in sterile PBS before injection.

GalNAc conjugated Anln siRNAs

These were obtained from Alnylam Pharmaceuticals. 10mg/ml stocks for si*Luc* and si*Anln* were stored at −20°C. The working concentration of the siRNA was 4mg/ml, diluted in PBS. For testing efficiency of siRNAs, we subcutaneously injected each of these GalNAc-siRNAs into wild-type mice at 1 mg/kg and liver tissues were collected 3 days later to assess knockdown efficiency by qPCR. After choosing the si*Anln* with best knockdown efficiency (si*Anln* #1), the subsequent experiments used a higher dose of 4 mg/kg. For regeneration experiments, siRNAs were injected weekly, and for DEN-induced HCC experiments, siRNAs were injected every other week.

Primary hepatocyte isolation and transplantation

Primary hepatocytes from B6 wild-type mouse were isolated by two-step collagenase perfusion. Liver perfusion medium (Thermo Fisher Scientific, 17701038), liver digest medium (Thermo Fisher Scientific, 17703034) and Hepatocyte wash medium (Thermo Fisher Scientific, 17704024) were used. Cell number and viability were determined by Trypan blue exclusion in a hemocytometer. Cells were re-suspended in DMEM (no FBS) at 1 million/100uL, and transplanted into *FRG* mice by splenic injection at 100uL/mouse.

Liver repopulation experiment in FRG mice

NTBC water was discontinued one day prior to hepatocyte transplantation and subsequently cycled (7 days off and 3 days on). Two days after transplantation, *FRG* mice were randomly divided into *GalNAc-siAnln* and *GalNAc-siLuc* treated groups, and the treatment was started. Body weights were measured twice every week. After 6 weeks of treatment, mice were sacrificed to examine levels of liver repopulation.

Histology, immunohistochemistry, and immunofluorescence

Tissue samples were fixed in 4% paraformaldehyde (PFA) and embedded in paraffin. In some cases, frozen sections were made. Immunohistochemistry was performed as previously

described [31]. For immunofluorescence staining, transfected cells were fixed in 4% paraformaldehyde (PFA) at 37C or 15min, followed by blocking with 5% BSA/0.25% Triton in PBS for 1h. Primary antibodies used: Cyp2e1 (Abcam, ab28146), Ctnnb1 (BD Transduction Laboratories #610154), Aurora B (Abcam ab2254), alpha-Tubulin (CST #3873). For immunohistochemistry, detection was performed with the Elite ABC Kit and DAB Substrate (Vector Laboratories), followed by Hematoxylin Solution counterstaining (Sigma). Images were taken by an Olympus IX83 microscope. H&E staining and trichrome staining were performed by the UTSW Histo Pathology Core Facility or the UTSW Tissue Procurement Service. H&E slides were interpreted by P.G., a clinical pathologist with expertise in human liver cancer.

RNA Extraction and qRT-PCR

Total RNA was isolated using TRIzol reagent (Invitrogen, #15596018). For qRT-PCR of miRNA or mRNA, cDNA synthesis was performed with 1 mg of total RNA using the miScript II reverse transcription kit (QIAGEN, #218161) or iScript RT Supermix (BioRad, #1708840). 12.5 ng of total RNA was used to measure mRNA expression levels via qRT-PCR. mRNA levels were normalized to β-Actin gene expression. Gene expression levels were measured using the ΔΔCt method as described previously [32].

Statistical Analysis

The data in most figure panels reflect multiple experiments performed on different days using mice derived from different litters. Variation is always indicated using standard error presented as mean ± SEM. Two-tailed Student's t-tests (two-sample equal variance) were used to test the significance of differences between two groups. Statistical significance is displayed as $p<0.05$ (*) or $p<0.01$ (**) unless specified otherwise. In all experiments, no mice were excluded form analysis after the experiment was initiated. Image analysis for the quantification was blinded.

RESULTS

Anln is required for cytokinesis

To find a specific target involved in cytokinesis, we first examined the results of a previously performed RNAi screen that identified essential cell cycle regulators[33]. We assessed four candidate genes associated with cytokinesis defects (*Incenp, Cdk1, Ect2,* and *Anln*). To determine which ones were required for cytokinesis in liver cells, we performed siRNA knockdowns in a SV40 transformed hepatocyte cell line called H2.35 (Supplementary Figure 1A). 72 hours after siRNA transfection, we performed flow cytometry to examine changes in cellular ploidy. *siAnln* transfected cells underwent much more dramatic increases in polyploidization (Supplementary Figure 1A, Figure 1A–B), thus we chose to focus exclusively on *Anln*. Further analysis with live imaging showed that *siAnln* cells failed to complete cytokinesis (Figure 1C), and became large and multinucleated (Figure 1D).

To further examine the precise stage at which *Anln* is essential, we used immunofluorescence to examine mitosis and cell division (Figure 1E). Aurora B kinase, used to identify distinct stages of mitosis, is co-localized at the invaginating cleavage furrow

during cytokinesis. siRNA treated cells were synchronized at the G2/M stage by nocodazole. After nocodazole was removed, Aurora B is localized to DNA in both siRNA groups at time 0 min. Both groups showed Aurora B localization at centromeres, marking relatively normal metaphase (40 min). At 80 min, *siScr* treated cells continued with normal anaphase and telophase, marked by localization of Aurora B at the cleavage furrow, while *siAnln* treated cells did not form a normal cleavage furrow, indicating a failure to enter anaphase/telophase. *siScr* cells completed cytokinesis at around 120 min, but *siAnln* treated cells still appeared to be frozen in anaphase and could not generate a cleavage furrow or contractile ring. 92% of *siScr* cells completed mitosis including cytokinesis, compared to 24% of *siAnln* cells (Figure 1F, n = 25–36 cells analyzed per group). These data demonstrated that dividing cells require normal levels of ANLN to complete cytokinesis.

ANLN is overexpressed in liver cancers and is associated with poor prognosis

To determine whether *ANLN* has important roles in human cancer, we examined *ANLN* expression in multiple malignancies. RNA-seq data from The Cancer Genome Atlas showed that *ANLN* mRNA expression is upregulated in most tumor types when compared to normal tissues (Figure 2A). In support of putative oncogenic activities, higher *ANLN* expression is known to correlate with higher metastatic frequency[34] and poorer prognosis[35] (Figure 2B, from www.proteinatlas.org and Figure 2C from www.prognoscan.org). We then focused on the liver specifically and analyzed data from Oncomine showing that *ANLN* was expressed 2-fold higher in 35 HCCs as compared to 10 normal adjacent liver tissues (Figure 2D). We confirmed this upregulation of *ANLN* mRNA in our own collected matching pairs of HCC and normal tissues (Figure 2E). Furthermore, an HCC tissue microarray showed that *ANLN* protein levels were significantly higher in tumors compared to normal liver tissues (Figure 2F).

In vivo Anln knockdown impaired MYC-induced liver tumorigenesis

To determine if *Anln* and cytokinesis are required for liver tumor development in an endogenous cancer model, we delivered *Anln* siRNA into the well-established *MYC* driven hepatoblastoma model[36]. This is an aggressive cancer model in which human *c-MYC* is overexpressed in the liver by withdrawing doxycycline (dox) water at the time of birth (Supplementary Figure 1B). This model has 100% penetrance and a median survival of approximately 50 days. To suppress *Anln* expression, we packaged *siAnln* or *siScr* in lipid nanoparticles[30] and injected the LNPs intravenously into *LAP-MYC* mice from p10 to p25 (Figure 3A). The 5A2-SC8 dendrimer LNP was selected due to its ability to deliver siRNAs to hepatocytes and tumor cells with minimal carrier-induced hepatotoxicity.[30] *Anln* mRNA levels were significantly reduced in normal liver tissues after the dosing regimen (Figure 3B). There was no difference in the liver to body weight ratios between *siScr* and si*Anln* groups at P34, which is when macroscopic liver tumors first appear in this model (Figure 3C). At P34, si*Anln* treated mice exhibited significantly fewer tumor nodules on gross and histologic examination (Figure 3D–F). Moreover, *siAnln* treated mice survived significantly longer (Figure 3G; $p < 0.05$). These results suggested that elevated *Anln* expression and cytokinesis are required for efficient transformation and tumor initiation in the *MYC*-induced hepatoblastoma model.

Anln suppression impaired tumor engraftment in a chronic liver damage model

To inhibit *Anln* expression in a temporally-specific and prolonged fashion, we developed a retroviral doxycycline (dox)-inducible Tet-on system to drive the expression of either scrambled (*shScr*) or *Anln* shRNA (*shAnln*) (Figure 4A, vector obtained from Scott Lowe's lab[37]). After testing 10 distinct *Anln* shRNAs, *shAnln* #2 and #3 were selected based on their knockdown efficiency (Figure 4B). Similar to siRNA experiments, H2.35 cells stably infected with *shAnln* #2 or #3 underwent polyploidization after three days of dox induction, indicating ongoing mitosis with cytokinesis failure (Figure 4C). To determine whether this retroviral system was truly inducible, we measured proliferation of cells stably infected with either *shScr* or *shAnln*. While there were no differences in proliferation in the absence of dox, *shAnln* 2 and 3 containing cells showed significant growth inhibition after dox exposure (Figure 4D).

We next tested the effects of *Anln* inhibition in a chronic liver damage model based on hereditary tyrosinemia[38]. Without treatment, the livers of fumarylacetoacetate hydrolase $(FAH)^{-/-}$; $Rag1^{-/-}$; $IL\text{-}2R\gamma^{-/-}$ (*FRG*) mice accumulate a toxic metabolite called fumarylacetoacetate, develop liver failure, and subsequently die. The injured liver microenvironment contributes to the development of cirrhosis and HCC[39]. To effectively treat this liver disease, mice and human patients are normally given NTBC (2-(2-nitro-4-trifluoromethylbenzoyl)-1,3-cyclohexanedione), a drug that clears fumarylacetoacetate and effectively maintains a healthy liver. Because *FRG* livers experience extensive hepatocyte destruction, these mice can be used as efficient transplant recipients for normal hepatocytes or HCC cells[38, 40, 41].

We transplanted the stably shRNA infected H2.35 cell lines into immunosuppressed *FRG* mice via splenic injection, which led to the homogenous delivery of cancer cells throughout the liver. This models widespread intrahepatic metastasis in the setting of chronic liver damage. After splenic transplantation, we withdrew NTBC to induce liver damage in host tissues, and kept half of the *shScr* and *shAnln* H2.35 transplanted mice on regular water and the other half on dox water to drive shRNA expression (Figure 4E). After 49 days, we found that the mice without dox induction had similar levels of tumorigenesis (Figure 4F). In contrast, the *shAnln* mice exposed to dox water had significantly fewer tumor nodules than the *shScr* mice (Figure 4F). GFP expression allowed us to detect greater clonal expansion of *shScr* donor cells (Figure 4G). These data collectively indicated that suppressing *Anln* could impair the engraftment and expansion of HCCs within a chronically injured liver disease model.

Anln suppression in transgenic mice prevented HCC formation in a DEN + CCl_4 model

The *MYC* experiment showed that *Anln* suppression was effective against hepatoblastoma development in a non-injured environment and the *FRG* experiment showed that *Anln* suppression was effective in a cell-autonomous fashion within a chronic liver injury model. Ultimately, the most critical question is whether or not potent *Anln* suppression in all cells of the liver would be safe and/or effective in a clinically relevant, chronic liver injury model. Towards these ends, we engineered a dox-inducible transgenic mouse expressing *shAnln* #2. Transgenic mice were derived from embryonic stem cells containing *Rosa-rtTA* and a GFP

expressing sh*Anln* cassette under the control of a tetracycline responsive promoter element (*TRE*) (Supplementary Figure 1C; transgenic design based on[26]). Dox could be used to induce shRNA and *Anln* suppression in a temporally specific fashion. *Rosa-rtTa* alone or *Rosa-rtTa; TRE-shAnln* (hereafter called *Rosa* and *TG-shAnln*) transgenic mice exposed to dox water from P0–P20 showed normal growth, development, and liver function. We had previously found that *Anln* mRNA levels were suppressed by 50% in this model resulting in hyperpolyploid livers after dox withdrawal[42]. This mouse model demonstrated that transient *Anln* suppression in vivo was sufficient to increase polyploidy.

We first tested the tumorigenesis in this model with DEN alone, and the *TG-shAnln* mice exhibited strong inhibition of tumor development (Supplementary Figure 1D). HCC in the western world most often arises in microenvironments characterized by chronic inflammation, fibrosis, and hepatocyte proliferation. In mice, this scenario can be mimicked by introducing DEN followed by biweekly carbon tetrachloride (CCl_4) to induce chronic injury[43]. We gave *Rosa* and *TG-shAnln* mice DEN at P15, exposed both cohorts to dox to induce *shAnln* in the experimental group starting at P32, then started biweekly CCl_4 injections at P39 (Figure 5A). After 8 weeks of CCl_4 injury, liver function tests revealed lower AST and ALT levels in *TG-shAnln* group (Supplementary Figure 1E). After 12 weeks of CCl_4, *TG-shAnln* mice exhibited almost no frank HCC development especially when compared to the multifocal disease seen in control mice (Figure 5B, C). Moreover, liver to body weight ratios were much higher in the *Rosa* group, likely due to the higher tumor burden (Figure 5C). Examination of liver histology showed similar levels of liver pathology as compared to control mice (Figure 5D). qPCR for fibrosis genes from the non-tumor compartment showed that *Col1a1* and *Col1a3* were modestly higher in *TG-shAnln* mice, suggesting a trend toward greater collagen deposition and fibrosis (Figure 5E). However, trichrome quantification revealed similar level of fibrosis in control and *TG-shAnln* livers (Figure 5F). Also, we did not identify a reduction in proliferation within *TG-shAnln* livers (Supplementary Figure 1F, G). Moreover, there was no significant difference in genotoxicity (Supplementary Figure 1H). These results showed that inhibiting cytokinesis almost completely blocked tumorigenesis in a chronic injury liver model without major effects on liver damage and repair.

Anln suppression in transgenic mice did not impair liver function or regeneration

Although *Anln* suppression could effectively inhibit liver cancer development in multiple settings, it was possible that it could also harm normal cells through the blockade of cytokinesis. To examine the effect of suppressing *Anln* on normal liver, we first assessed liver gene expression after *Anln* suppression and cytokinesis inhibition. There was no significant impact on liver differentiation gene expression after *shAnln* induction from P0–P20 (Figure 6A and B). This is also corroborated by Glutamine synthetase and Cyp2e1 immunostaining on control and *Anln* suppressed liver tissues (Figure 6C). Although suppression of *Anln* did not cause liver damage or changes in cellular differentiation, we hypothesized that there might be negative effects on cell growth and regeneration after injury, since induction of *shAnln* led to downregulation of cell cycle genes in the *TG-shAnln* livers (Supplementary Figure 1I). After partial hepatectomy in adult *Rosa* and *TG-shAnln* mice that had been induced with dox for one week, we saw no differences in liver to body

weight ratios after 40 hours, 3 days and 7 days of regeneration (Figure 6D). There were similar numbers of mitotic cells as detected by phospho-H3 (Figure 6E–G). Likewise, expression of cell cycle genes was unchanged (Supplementary Figure 2A). *TG-shAnln* livers did exhibit significantly larger hepatocytes 7 days after surgery (Supplementary Figure 2B–E). After we challenged mice with two doses of CCl_4, *TG-shAnln* mice did not exhibit higher AST or ALT levels compared to control mice (Figure 6H). Together, these data demonstrated that suppression of *Anln* and cytokinesis did not have a detrimental impact on liver regeneration after acute injuries.

GalNAc mediated siAnln delivery inhibited cancer but did not impair liver regeneration

Even after performing toxicity experiments in *Rosa-rtta* induced shRNA transgenic mice, we still had questions regarding long-term safety. First, it was unclear if the whole-body shRNA expression in the *TG-shAnln* might have potentially masked liver damage via the knockdown of *Anln* in other cell types (lymphocytes, for example). In addition, it is well known that shRNAs can cause liver toxicity in part due to high-dose mediated saturation of endogenous microRNA processing machinery. Moreover, LNPs that are used to package siRNAs can cause toxicity independent of the target, an issue that we previously studied in the context of improved LNP development.[30] To circumvent some of these concerns, we asked if we could safely and effectively block liver cancer using an alternative small RNA delivery strategy, which involves attaching N-acetylgalactosamine (GalNAc) to nucleic acid molecules. Hepatocytes express the Asialoglycoprotein receptor (ASGPR), which mediate the uptake and clearance of circulating glycoproteins with exposed GalNAc. These siRNA reagents would allow us to test potential effects of hepatocyte-specific knockdown at clinically achievable doses.

23 different siRNAs against *Anln* were screened using a luciferase based platform. Six of the best siRNAs against *Anln* and a control siRNA against firefly luciferase (si*Luc*) were then GalNAc-conjugated. After in vivo testing, siRNA #1 (hereafter referred to as si*Anln* or GalNAc-*siAnln*) was selected for subsequent in vivo experiments (Supplementary Figure 3A). Consistent with the *TG-shAnln* model, the GalNAc-*siAnln* treated livers did not show altered expression of differentiation markers (Supplementary Figure 3B).

We then tested liver regeneration after GalNAc-si*Anln* using a panel of liver injury models. We first challenged the mice with partial hepatectomy and harvested livers at 40h, 3 days, and 7 days after surgery. No differences in liver to body weight ratios between si*Luc* and si*Anln* treated mice were detected at any time points (Figure 7A and B). Mitosis rates were also similar, as assessed by phospho-H3 (Supplementary Figure 3C–E). Next, we used CCl_4 to test regeneration under both acute and chronic injuries. Again, we started the weekly siRNA (4 mg/kg) 1 week prior to CCl_4, which was given twice per week chronically. si*Anln* treated mice failed to show higher AST, ALT and TBIL after acute (1 week) or chronic (6 weeks) CCl_4 injury (Figure 7C and Supplementary Figure 4B). Albumin and glucose in si*Anln* treated mice were slightly lower than controls after 8 weeks of CCl_4 (Figure 4A, C), but these parameters were still within normal limits. Moreover, cell cycle genes were similarly expressed between the two groups (Supplementary Figure 4D), suggesting unimpaired liver regeneration. As an indication of cytokinesis inhibition and siRNA efficacy,

GalNAc-siAnln treated livers possessed larger hepatocytes as compared to controls (Supplementary Figure 4E, F).

We then used the *FRG* hepatocyte transplantation system to more stringently test hepatocyte proliferation in the setting of *Anln* suppression. Because the transplanted hepatocytes are required to proliferate multiple rounds in order to repopulate the *FRG* liver, this model exerts a greater demand on proliferation. *FRG* recipients of wild-type primary hepatocytes were treated with weekly GalNAc-si*Luc* or GalNAc-si*Anln* (4 mg/kg). The GalNAc-si*Anln* treated mice exhibited similar body weights compared to controls (Figure 7D). 45 days after transplantation, the body, liver, and liver/body weight ratios were unchanged (Figure 7F). Hepatocyte repopulation efficiency as measured by FAH IHC was similar between groups (Figure 7E). Furthermore, *Anln* knockdown was confirmed and cell cycle gene expression was unchanged (Supplementary Figure 4G, H). Finally, we confirmed the efficacy of GalNAc-si*Anln* on DEN-mediated and *LAP-MYC* tumorigenesis (Figure 7G, H), suggesting that GalNAc-*siAnln* delivery is able to inhibit tumors in multiple settings. Taken together, these results demonstrated that suppression of *Anln* was able to effectively inhibit HCC but did not significantly impair liver regeneration after acute and chronic injuries.

DISCUSSION

Acute liver regeneration and cancer both depend on cellular growth and proliferation mechanisms. It is unclear if regeneration during chronic injury is as dependent on these mechanisms, since cell turnover is less dramatic than it is during acute tissue damage. It is also unknown if cancer is more or less dependent on these growth mechanisms. In the normal liver, tissue and cell growth can occur even when cytokinesis is impaired. This occurs when hepatocytes polyploidize after weaning and it occurs to an extreme extent in mutant models with mitosis and cytokinesis defects[14]. This ability to tolerate cytokinesis inhibition begs the question about the requirements for cytokinesis in the context of chronic liver damage, where there is an ongoing demand for cell division.

In this study, we used in vitro and in vivo models to determine if there is a therapeutic window for cytokinesis inhibition in several real-world contexts where liver cancer arises. As previously reported for other genes, we find that acute regeneration does not require completely intact cell division or cytokinesis, likely because only small increases in cellular mass are needed. As expected, it appeared that liver cancers such as hepatoblastoma and HCC were highly dependent on cytokinesis. Although polyploid genomes are observed in cancer, a continuous increase in ploidy did not permit cells to transform or clonally expansion in the models used. The therapeutic index could also be increased due to the ability to deliver siRNAs in a liver specific fashion, since the liver is potentially more able to tolerate incomplete cytokinesis than other tissues. This might represent an advantage for small RNA therapies that only efficiently target the liver over small molecules that result in toxicity in multiple tissues.

A more complex challenge presents itself when one imagines cytokinesis inhibition for HCCs that arise in the setting of chronic liver damage. Given the possibility that regeneration over longer time courses might require normal cytokinesis, it is possible that

Anln suppression would not be tolerated even if it were effective against HCC formation. We were surprised to find continued survival and a lack of worsening hepatitis in *Anln* suppressed and CCl_4 exposed mice. Because knockdown of *Anln* was not 100%, it is possible that partial cytokinesis inhibition permitted chronic regeneration but was enough to prevent HCC development. This suggests an adequate therapeutic window for cancer prevention. It was possible that the chronic shRNA expression in *TG-shAnln* transgenic mice might be toxic due to shRNA overexpression rather than any on target effects. However, the tests with GalNAc-siRNAs indicated that suppressing *Anln* will likely be well tolerated in terms of liver damage. It is unclear if GalNAc-based approaches will be effective as a preventative therapy, given the inability of GalNAc to target HCC cells, but our study provides a pre-clinical proof of concept to motivate further examination of cytokinesis inhibition in patients at high risk for HCC development. Within the 1–3 years after "curative" interventions such as resection, ablative techniques, or radiation therapy, there is a high risk for recurrence or de novo HCC[44]. One could imagine using *ANLN* suppression as an adjuvant treatment after such therapeutic interventions. We believe that cytokinesis inhibition could prevent transformation in these pre-malignant hepatocytes that are within a damaged liver "field".

Supplementary Material

Refer to Web version on PubMed Central for supplementary material.

Acknowledgments

Grant support

H.Z. was supported by the Pollack Foundation, an American Cancer Society pilot grant, a NIH/NCI R01 grant (1R01CA190525), a Burroughs Welcome Career Medical Award, and a CPRIT New Investigator grant (R1209). D.J.S. was supported by CPRIT (R1212), the Welch Foundation (I-1855), and the American Cancer Society (RSG-17-012-01).

We thank the Alnylam's Bioinformatics, Oligo synthesis and RNAi Lead Discovery team for designing, generating and screening for the Anln GalNAc siRNAs.

References

1. Barr FA, Gruneberg U. Cytokinesis: placing and making the final cut. Cell. 2007; 131:847–60. [PubMed: 18045532]
2. Fujiwara T, Bandi M, Nitta M, et al. Cytokinesis failure generating tetraploids promotes tumorigenesis in p53-null cells. Nature. 2005; 437:1043–7. [PubMed: 16222300]
3. Pampalona J, Frias C, Genesca A, et al. Progressive telomere dysfunction causes cytokinesis failure and leads to the accumulation of polyploid cells. PLoS Genet. 2012; 8:e1002679. [PubMed: 22570622]
4. Lv L, Zhang T, Yi Q, et al. Tetraploid cells from cytokinesis failure induce aneuploidy and spontaneous transformation of mouse ovarian surface epithelial cells. Cell Cycle. 2012; 11:2864–75. [PubMed: 22801546]
5. Hognas G, Tuomi S, Veltel S, et al. Cytokinesis failure due to derailed integrin traffic induces aneuploidy and oncogenic transformation in vitro and in vivo. Oncogene. 2012; 31:3597–3606. [PubMed: 22120710]
6. Duncan AW. Aneuploidy, polyploidy and ploidy reversal in the liver. Semin Cell Dev Biol. 2013; 24:347–56. [PubMed: 23333793]

7. Duncan AW, Newell AEH, Smith L, et al. Frequent Aneuploidy Among Normal Human Hepatocytes. Gastroenterology. 2012; 142:25–28. [PubMed: 22057114]
8. Duncan AW, Taylor MH, Hickey RD, et al. The ploidy conveyor of mature hepatocytes as a source of genetic variation. Nature. 2010; 467:707–U93. [PubMed: 20861837]
9. Gentric G, Desdouets C, Celton-Morizur S. Hepatocytes polyploidization and cell cycle control in liver physiopathology. Int J Hepatol. 2012; 2012:282430. [PubMed: 23150829]
10. Celton-Morizur S, Merlen G, Couton D, et al. The insulin/Akt pathway controls a specific cell division program that leads to generation of binucleated tetraploid liver cells in rodents. Journal of Clinical Investigation. 2009; 119:1880–1887. [PubMed: 19603546]
11. Margall-Ducos G, Celton-Morizur S, Couton D, et al. Liver tetraploidization is controlled by a new process of incomplete cytokinesis. Journal of Cell Science. 2007; 120:3633–3639. [PubMed: 17895361]
12. Simson IW. Polyploid, aneuploid and multinucleate cells in the human liver. J Pathol Bacteriol. 1963; 85:35–9. [PubMed: 13977577]
13. Duncan AW, Hanlon Newell AE, Smith L, et al. Frequent aneuploidy among normal human hepatocytes. Gastroenterology. 2012; 142:25–8. [PubMed: 22057114]
14. Diril MK, Ratnacaram CK, Padmakumar VC, et al. Cyclin-dependent kinase 1 (Cdk1) is essential for cell division and suppression of DNA re-replication but not for liver regeneration. Proceedings of the National Academy of Sciences of the United States of America. 2012; 109:3826–3831. [PubMed: 22355113]
15. Hickson GR, O'Farrell PH. Anillin: a pivotal organizer of the cytokinetic machinery. Biochem Soc Trans. 2008; 36:439–41. [PubMed: 18481976]
16. Piekny AJ, Maddox AS. The myriad roles of Anillin during cytokinesis. Semin Cell Dev Biol. 2010; 21:881–91. [PubMed: 20732437]
17. Piekny AJ, Glotzer M. Anillin is a scaffold protein that links RhoA, actin, and myosin during cytokinesis. Current Biology. 2008; 18:30–36. [PubMed: 18158243]
18. D'Avino PP, Archambault V, Przewloka MR, et al. Isolation of protein complexes involved in mitosis and cytokinesis from Drosophila cultured cells. Methods Mol Biol. 2009; 545:99–112. [PubMed: 19475384]
19. Oegema K, Savoian MS, Mitchison TJ, et al. Functional analysis of a human homologue of the Drosophila actin binding protein anillin suggests a role in cytokinesis. J Cell Biol. 2000; 150:539–52. [PubMed: 10931866]
20. Field CM, Alberts BM. Anillin, a contractile ring protein that cycles from the nucleus to the cell cortex. J Cell Biol. 1995; 131:165–78. [PubMed: 7559773]
21. Giansanti MG, Bonaccorsi S, Gatti M. The role of anillin in meiotic cytokinesis of Drosophila males. Journal of Cell Science. 1999; 112:2323–2334. [PubMed: 10381388]
22. Oegema K, Savoian MS, Mitchison TJ, et al. Functional analysis of a human homologue of the Drosophila actin binding protein anillin suggests a role in cytokinesis. Journal of Cell Biology. 2000; 150:539–551. [PubMed: 10931866]
23. Zhou W, Wang Z, Shen N, et al. Knockdown of ANLN by lentivirus inhibits cell growth and migration in human breast cancer. Mol Cell Biochem. 2015; 398:11–9. [PubMed: 25223638]
24. Suzuki C, Daigo Y, Ishikawa N, et al. ANLN plays a critical role in human lung carcinogenesis through the activation of RHOA and by involvement in the phosphoinositide 3-kinase/AKT pathway. Cancer Res. 2005; 65:11314–25. [PubMed: 16357138]
25. Magnusson K, Gremel G, Ryden L, et al. ANLN is a prognostic biomarker independent of Ki-67 and essential for cell cycle progression in primary breast cancer. Bmc Cancer. 2016:16. [PubMed: 26758745]
26. Premsrirut PK, Dow LE, Kim SY, et al. A rapid and scalable system for studying gene function in mice using conditional RNA interference. Cell. 2011; 145:145–58. [PubMed: 21458673]
27. Zuber J, McJunkin K, Fellmann C, et al. Toolkit for evaluating genes required for proliferation and survival using tetracycline-regulated RNAi. Nature Biotechnology. 2011; 29:79.
28. Beer S, Komatsubara K, Bellovin DI, et al. Hepatotoxin-induced changes in the adult murine liver promote MYC-induced tumorigenesis. PLoS One. 2008; 3:e2493. [PubMed: 18560566]

29. Mitchell C, Willenbring H. A reproducible and well-tolerated method for 2/3 partial hepatectomy in mice. Nat Protoc. 2008; 3:1167–70. [PubMed: 18600221]
30. Zhou K, Nguyen LH, Miller JB, et al. Modular degradable dendrimers enable small RNAs to extend survival in an aggressive liver cancer model. Proceedings of the National Academy of Sciences of the United States of America. 2016; 113:520–525. [PubMed: 26729861]
31. Zhu H, Shah S, Shyh-Chang N, et al. Lin28a transgenic mice manifest size and puberty phenotypes identified in human genetic association studies. Nat Genet. 2010; 42:626–30. [PubMed: 20512147]
32. Zhu H, Shyh-Chang N, Segre AV, et al. The Lin28/let-7 axis regulates glucose metabolism. Cell. 2011; 147:81–94. [PubMed: 21962509]
33. Kittler R, Pelletier L, Heninger AK, et al. Genome-scale RNAi profiling of cell division in human tissue culture cells. Nat Cell Biol. 2007; 9:1401–12. [PubMed: 17994010]
34. Hall PA, Todd CB, Hyland PL, et al. The septin-binding protein anillin is overexpressed in diverse human tumors. Clin Cancer Res. 2005; 11:6780–6. [PubMed: 16203764]
35. Wang G, Shen W, Cui L, et al. Overexpression of Anillin (ANLN) is correlated with colorectal cancer progression and poor prognosis. Cancer Biomark. 2016; 16:459–65. [PubMed: 27062703]
36. Shachaf CM, Kopelman AM, Arvanitis C, et al. MYC inactivation uncovers pluripotent differentiation and tumour dormancy in hepatocellular cancer. Nature. 2004; 431:1112–7. [PubMed: 15475948]
37. Zuber J, McJunkin K, Fellmann C, et al. Toolkit for evaluating genes required for proliferation and survival using tetracycline-regulated RNAi. Nat Biotechnol. 2011; 29:79–83. [PubMed: 21131983]
38. Azuma H, Paulk N, Ranade A, et al. Robust expansion of human hepatocytes in Fah(−/−)/Rag2(−/−)/Il2rg(−/−) mice. Nature Biotechnology. 2007; 25:903–910.
39. Budhu A, Forgues M, Ye QH, et al. Prediction of venous metastases, recurrence, and prognosis in hepatocellular carcinoma based on a unique immune response signature of the liver microenvironment. Cancer Cell. 2006; 10:99–111. [PubMed: 16904609]
40. Shafritz DA. A human hepatocyte factory. Nat Biotechnol. 2007; 25:871–2. [PubMed: 17687361]
41. Grompe M, Strom S. Mice with human livers. Gastroenterology. 2013; 145:1209–14. [PubMed: 24042096]
42. ZSZKLXLLNLZYTBSDaZ H. The polyploid state plays a tumor suppressive role in the liver. Biorxiv. 2017
43. Mu X, Espanol-Suner R, Mederacke I, et al. Hepatocellular carcinoma originates from hepatocytes and not from the progenitor/biliary compartment. J Clin Invest. 2015; 125:3891–903. [PubMed: 26348897]
44. Saraswat VA, Pandey G, Shetty S. Treatment algorithms for managing hepatocellular carcinoma. J Clin Exp Hepatol. 2014; 4:S80–9. [PubMed: 25755616]

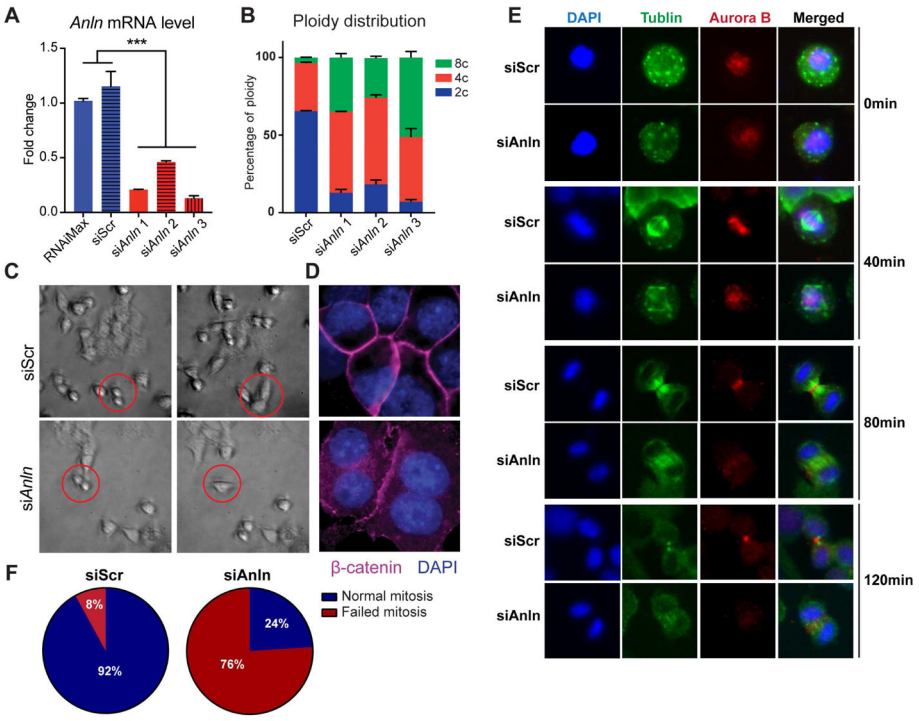

Figure 1. *Anln* is a cytokinesis regulator and is required for cytokinesis

(A) *Anln* mRNA levels in H2.35 cells after siRNA knockdown, as measured by RT-qPCR. si*Anln* #1 was selected for subsequent animal experiments.

(B) Ploidy distribution in H2.35 cells treated with either *siScr* or 3 different *Anln* siRNAs.

(C) Live imaging of H2.35 cells treated with either siScr or si*Anln* #1. Red circles are around cells undergoing or attempting division. Live imaging initiated 36 hours after transfection. Images were taken every 3 min. Videos are included in the Supplemental materials.

(D) DAPI and Ctnnb1 immunofluorescence staining of *siScr* and *siAnln* treated H2.35 cells. DAPI marks nuclei and Ctnnb1 marks cell membranes.

(E) Immunofluorescence staining for DAPI (blue), tubulin (green) and Aurora B (red) in H2.35 cells during mitosis. H2.35 cells were transfected with siScr or siAnln. 36 hours after transfection, cells were blocked with 150ng/mL nocodazole for 8 hours, washed, then given fresh media. Immediately after changing to fresh media, the time lapse started, and the cells were fixed with PFA in every 20 min for 140 min. The cells were then subjected to immunofluorescence staining.

(F) Quantification of normal mitotic events. 25–36 cells were counted for each group. Only cells in anaphase and telophase/cytokinesis (80 min and later) were included.

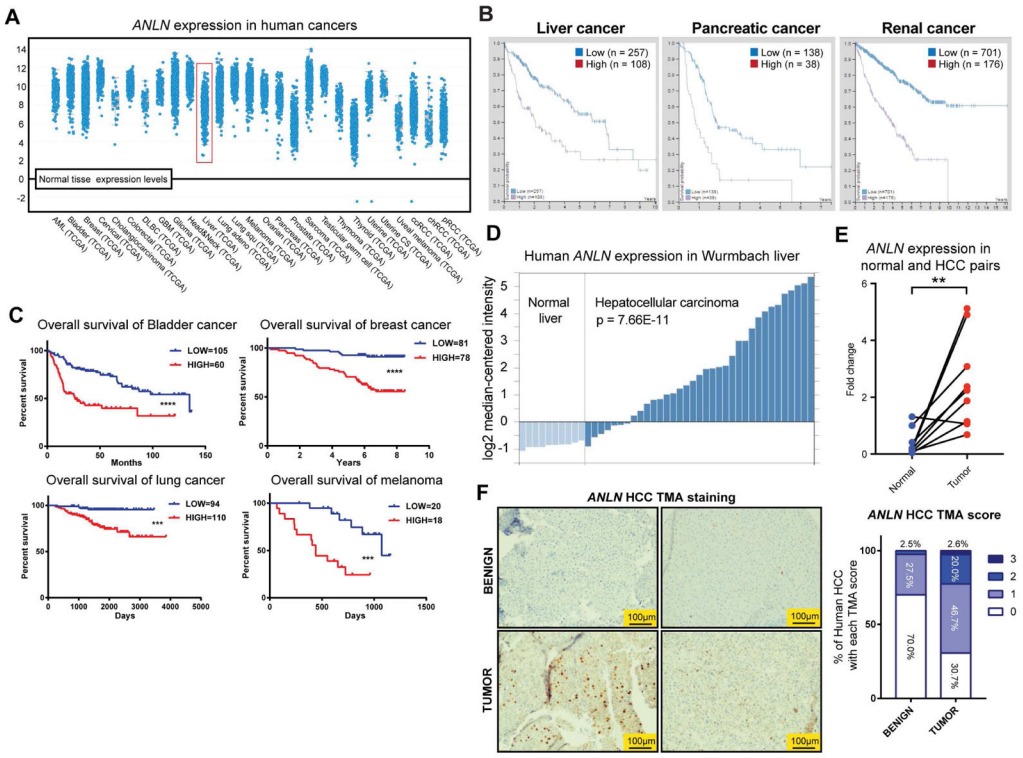

Figure 2. *ANLN* is overexpressed in liver cancers and is associated with poor prognosis

(A) Human *ANLN* expression in different tumor types from the TCGA database. Adapted from cBioPortal: http://www.cbioportal.org/index.do.

(B) Overall survival for patients with high and low *ANLN* expression in liver, pancreatic and renal cancers (https://www.proteinatlas.org).

(C) Overall survival curves for patients with high and low *ANLN* expression in bladder, breast, lung, and skin cancers. Adapted from http://www.abren.net/PrognoScan/.

(D) Human ANLN mRNA expression levels in normal liver and HCC tissues (Oncomine).

(E) RT-qPCR data showing human *ANLN* expression in matched normal and HCC pairs.

(F) ANLN HCC tissue microarray with 48 tumors and matching benign tissues. The *ANLN* expression level was scored based on the staining: 0: not detected; 1: low; 2: medium; 3: high. The percentage of human HCC with each TMA score is shown on the right.

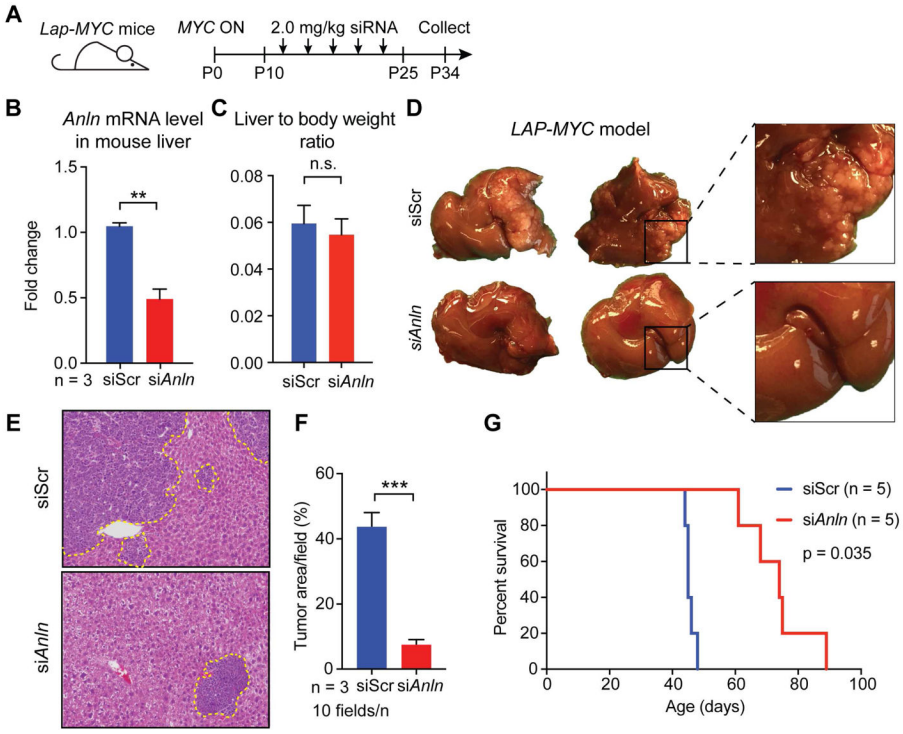

Figure 3. In vivo *Anln* knockdown impaired *MYC*-induced liver tumorigenesis

(A) A schematic of the induction and treatment regimen. Dox was withdrawn at P0 to induce human c-*MYC* expression. IV delivery (two intraperitoneal and three retro-orbital) of in vivo siRNAs packaged in LNPs started at P10 and lasted until P25. Dosing was twice per week at 2 mg/kg.

(B) *Anln* mRNA levels as determined by RT-qPCR in *MYC*-induced livers treated with either in vivo *siScr* or *siAnln*.

(C) Liver-to-body weight ratios of *MYC*-induced mice treated with either in vivo *siScr* or *siAnln* at P34.

(D) Gross liver images of *MYC*-induced mice treated with either in vivo *siScr* or *siAnln* at P34. Macroscopic tumors were observed in *siScr* but not in *siAnln* treated livers.

(E) H&E staining showing microscopic cancer lesions (circled by yellow dotted lines).

(F) Quantification of tumor area/field in the H&E staining in both siScr and si*Anln* treated mice. 10 random fields per mouse (n = 3 mice) were analyzed.

(G) Kaplan-Meier survival of *MYC*-induced mice treated with either in vivo *siScr* or *siAnln*.

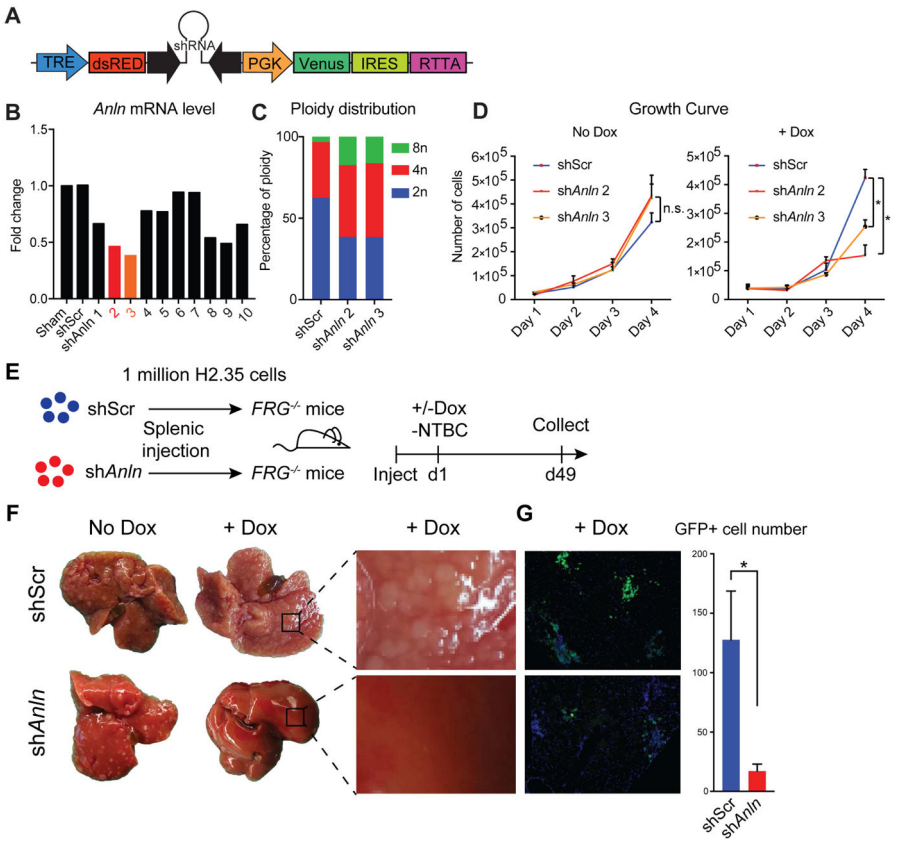

Figure 4. *Anln* suppression impaired tumor engraftment in a chronic liver damage model

(A) Retroviral TRMPVIR construct.

(B) To screen for knockdown efficiency of 10 distinct *shAnln's*, *Anln* mRNA levels in H2.35 cells were measured by RT-qPCR.

(C) Ploidy distribution in H2.35 cells treated with either *shScr*, *shAnln* #2, or *shAnln* #3.

(D) Proliferation assays in uninduced and dox-induced H2.35 cells containing either *shScr*, *shAnln* #2, or *shAnln* #3.

(E) A schematic of the *FRG* transplantation experiment.

(F) Gross images of *FRG* livers transplanted with either *shScr* or *shAnln* with or without dox induction.

(G) On the left are fluorescent images showing GFP+ H2.35 donor clones stably infected with either *shScr* or *shAnln*. On the right is the quantification of GFP+ H2.35 cells per field, 5 fields for each liver.

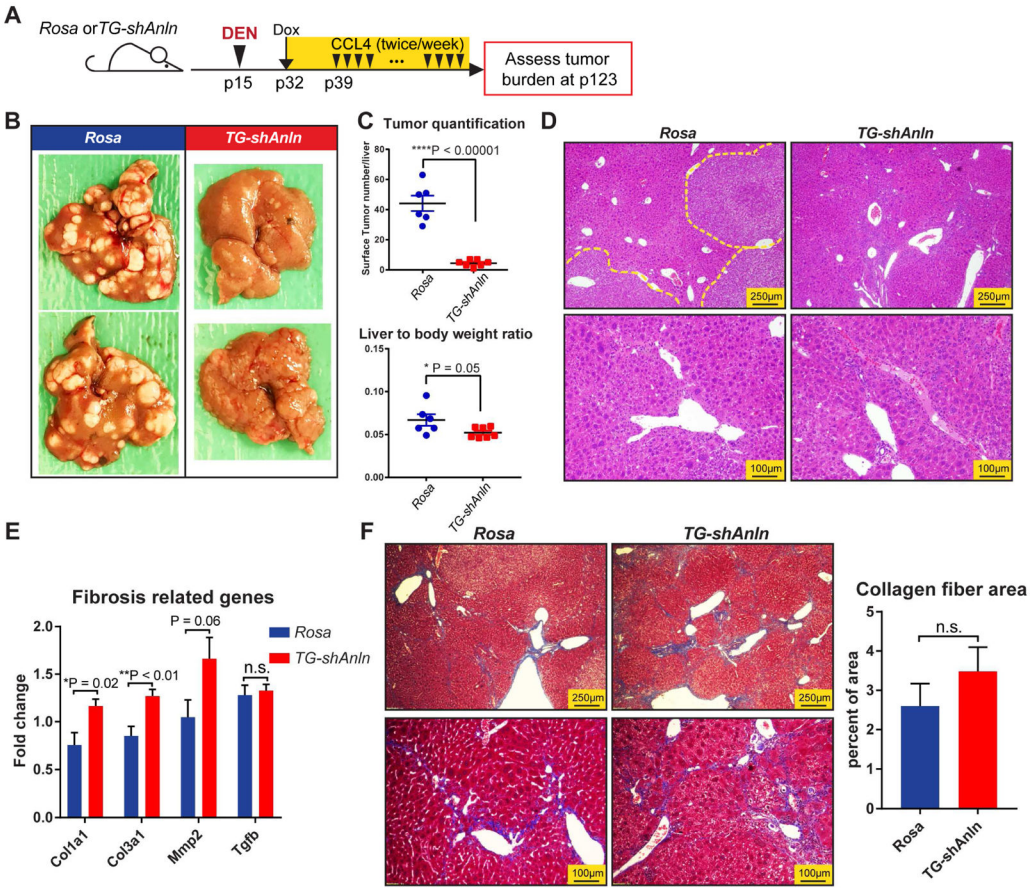

Figure 5. *Anln* suppression in transgenic mice prevented HCC formation in a DEN + CCl_4 model

(A) Schema for the DEN + chronic CCl_4 mediated HCC experiment in inducible shRNA mice. At P15, mice were injected with DEN (25μg/g). At P32, dox was started and one week later (P39), twice per week IP CCl_4 injections were started. Tumor burden was examined after 12 weeks of chronic CCl_4 injury (24 total doses).

(B) Representative gross tumor burden from *Rosa* and *TG-shAnln* mice.

(C) Liver surface tumor quantification and liver to body weight ratios.

(D) H&E histology of *Rosa* and *TG-shAnln* livers show tumor nodules (circled by dashed yellow outlines).

(E) qPCR for fibrosis related genes in *Rosa* and *TG-shAnln* livers as described in (A) (n = 6 mice per group).

(F) Trichrome staining showing collagen deposition in *Rosa* and *TG-shAnln* livers. On the right, quantification of trichrome+ areas (n = 4 mice in each group, 3 liver fragments were taken from each mouse, and 3 images were taken from each liver fragment, a total of 36 images examined per treatment group).

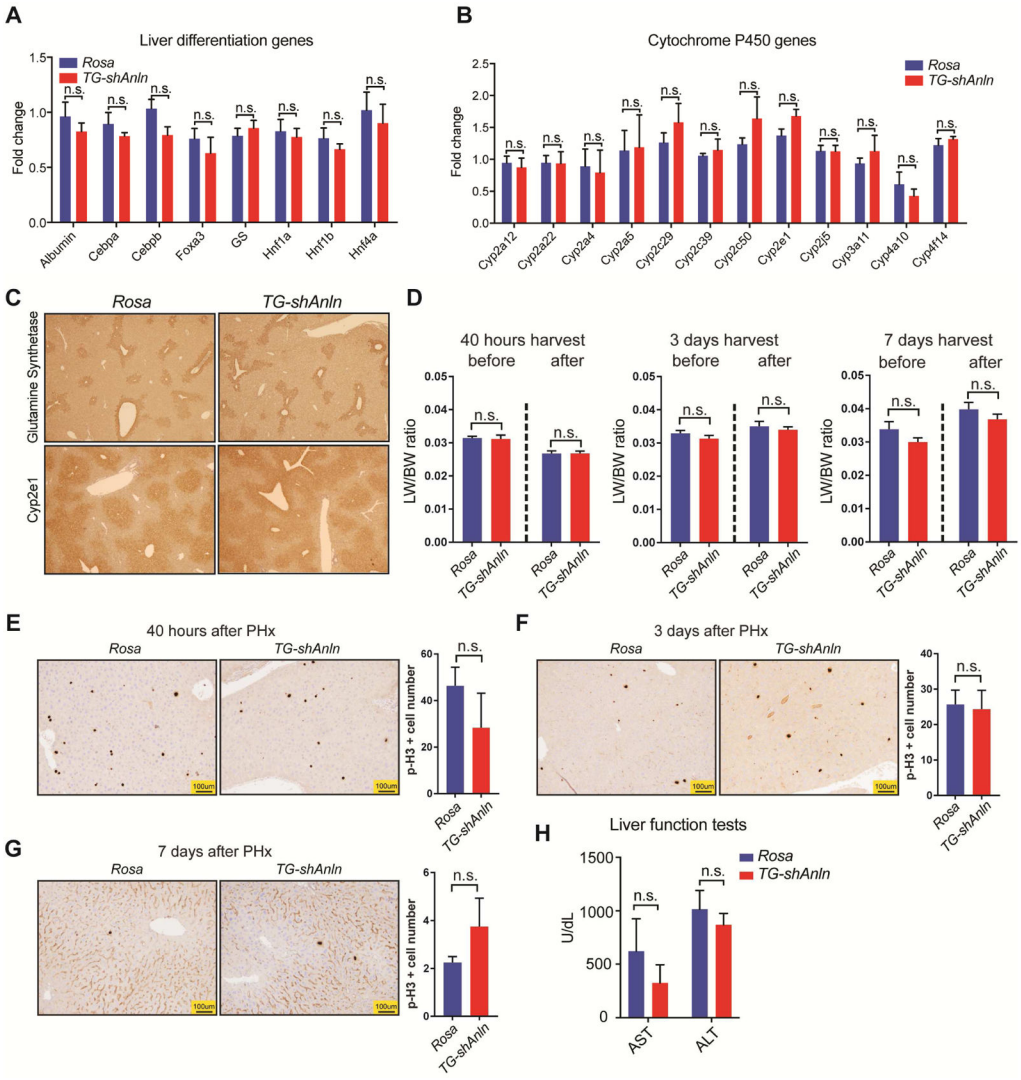

Figure 6. *Anln* suppression in transgenic mice did not impair liver function or regeneration

(A) qPCR for liver specific differentiation genes and transcription factors in *Rosa* and *TG-shAnln* livers (n = 5 per group). *Rosa* and *TG-shAnln* mice were given dox water (1g/L) after birth at P0 until P21, when livers were harvested.

(B) qPCR for Cytochrome P450 genes in *Rosa* and *TG-shAnln* livers (n = 5 per group).

(C) Glutamine synthetase (upper) and Cyp2e1 staining (lower panels) in *Rosa* and *TG-shAnln* livers.

(D) Liver to body weight ratios of regenerating livers at 40 hours, 3 days and 7 days after partial hepatectomy. Six week old *Rosa* and *TG-shAnln* mice were given dox for 7 days before surgery, then underwent 70% partial hepatectomy and remnant livers were harvested and analyzed at 40 hours, 3 days and 7 days after surgery (n = 3 mice per group for the 40-hour and 3-day time points, n = 4 for 7 day time point).

(E) Phospho-H3 staining in *Rosa* and *TG-shAnln* livers at 40 hours,

(F) 3 days, and

(G) 7 days after hepatectomy. Quantifications are shown on the right.

(H) Liver function tests of *Rosa* and *TG-shAnln* mice after two doses of CCl_4 given 3 days apart. The mice were induced with dox water (1g/L) one week before the first CCl_4 injection (n = 7 and 7).

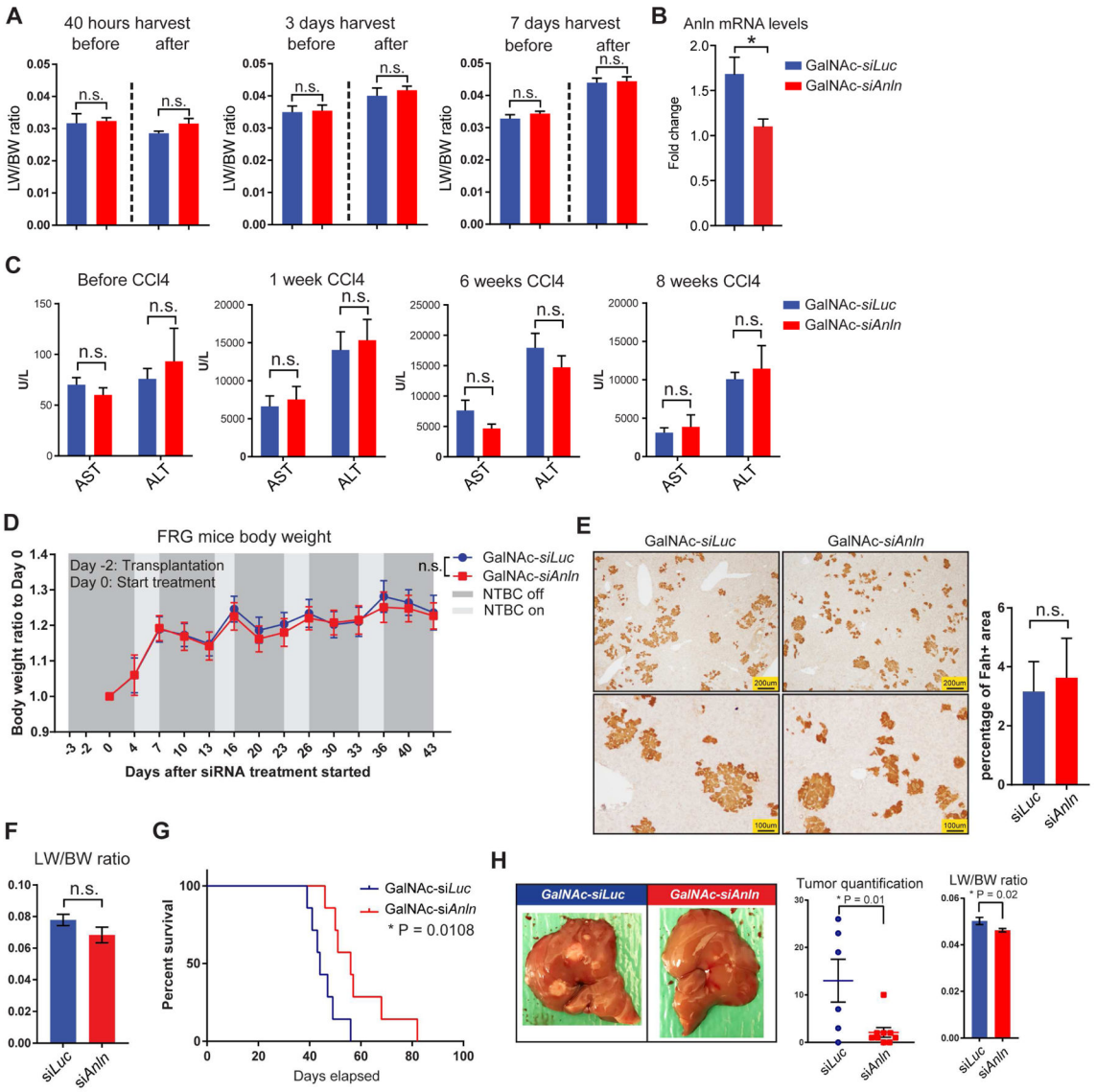

Figure 7. GalNAc mediated siAnln delivery inhibited cancer but did not impair liver regeneration

(A) Liver to body weight ratios of resected and regenerated livers after partial hepatectomy. Six-week old CD1 mice were given GalNAc-si*Luc* or GalNAc-si*Anln* (4mg/kg) 1 week before surgery, then underwent 70% partial hepatectomy. Remnant livers were harvested and analyzed at 40 hours, 3 days and 7 days after surgery (n = 3–5 per group).

(B) *Anln* mRNA levels of the above mice, as measured by qPCR.

(C) Liver function tests of mice before and after 1, 6, and 8 weeks of twice weekly CCl_4 injections. Mice were treated with weekly GalNAc-si*Luc* or GalNAc-si*Anln* (4mg/kg) (n = 7) starting 1 week before injury.

(D) Body weights of *FRG* mice over 45 days of siRNA treatments. *FRG* mice received 1×10^6 primary hepatocytes from wild-type B6 mice. Two days after transplantation, mice were randomly divided into weekly GalNAc-si*Luc* (4mg/kg, n = 6) and GalNAc-si*Anln* (4mg/kg, n = 7) treated groups. The mice were put on a NTBC water cycle (7 days without

NTBC followed by 3 days with NTBC), starting one day before transplantation. The Y-axis shows the ratio of the current body weight relative to the initial body weight.

(E) FAH immunostaining. The percentages of the FAH positive areas are quantified on the right (n = 4).

(F) Liver to body weight ratios of *FRG* mice after 45 days of siRNA treatment.

(G) Kaplan-Meier survival of *MYC*-induced mice treated with either GalNAc-*siLuc* or GalNAc-*siAnln. Lap-MYC* mice were taken off dox (*MYC* on) at birth. 4 mg/kg weekly siRNA treatments started at P8–P10 (n = 7).

(H) Representative tumor burden from C3h mice (left). C3h mice were given one dose of DEN (75ug/g) at P26. At P57, they were randomized to GalNAc-si*Luc* (4 mg/kg, n = 6) or GalNAc-si*Anln* (4 mg/kg, n = 9) groups, and started to receive siRNA treatment every two weeks. Mice were sacrificed at P230. On the right is the surface tumor quantification and liver to body weight ratios.